





Article

Manganese(I) Diamine Electrocatalysts: Electrochemical Carbon Dioxide Reduction to Carbon Monoxide

Badrinath Dhakal ¹, Brooke A. Corbin ¹, Alberto Sosa Parada ², Jonathan G. Sakai ², Emily A. Felton ³, Lauren T. McDonald ², Anthony J. Gross ², Gary S. Nichol ⁴ and Greg A. N. Felton ^{2,*}¹ Department of Chemistry, Oakland University, Rochester, MI 48309, USA² Department of Chemistry, Eckerd College, St. Petersburg, FL 33711, USA³ Department of Biology, University of Tampa, Tampa, FL 33606, USA⁴ School of Chemistry, University of Edinburgh, Edinburgh EH9 3FJ, UK

* Correspondence: feltonga@eckerd.edu

Abstract: Novel organometallic complexes Mn(benzene-1,2-diamine)(CO)₃Br, **Mn-1**, Mn(3-methylbenzene-1,2-diamine)(CO)₃Br, **Mn-2**, and Re(benzene-1,2-diamine)(CO)₃Cl, **Re-1**, have been synthesized and characterized by IR, UV/Vis, ¹H-NMR, EA and HRMS. The structures of **Mn-2** and **Re-1** were confirmed by X-ray crystallography. The three novel compounds were studied for their electrocatalytic reduction of carbon dioxide to carbon monoxide using cyclic voltammetry in acetonitrile solutions. Controlled potential electrolysis was used to obtain information on faradaic yield, with product formation being confirmed by GC. Using earth-abundant manganese, compounds **Mn-1** and **Mn-2** display turnover frequencies of 108 s⁻¹ and 82 s⁻¹, respectively, amid selective production of carbon monoxide (faradaic yields ~85%), with minimal co-production of dihydrogen (<2%), and low overpotential of 0.18 V. The rhenium congener, **Re-1**, displays no activity as an electrocatalyst for carbon dioxide reduction under identical conditions.

Keywords: CO₂ reduction; electrocatalyst; diamine; manganese compounds; CO formation



Citation: Dhakal, B.; Corbin, B.A.; Sosa Parada, A.; Sakai, J.G.; Felton, E.A.; McDonald, L.T.; Gross, A.J.; Nichol, G.S.; Felton, G.A.N. Manganese(I) Diamine Electrocatalysts: Electrochemical Carbon Dioxide Reduction to Carbon Monoxide. *Inorganics* **2023**, *11*, 374. <https://doi.org/10.3390/inorganics11090374>

Academic Editors: Francis Verpoort, Claudio Pettinari, Maurizio Peruzzini, Richard Layfield, Rainer Winter, Moris S. Eisen, Gábor Papp, Shuang Xiao and Axel Klein

Received: 1 September 2023

Revised: 18 September 2023

Accepted: 20 September 2023

Published: 21 September 2023



Copyright: © 2023 by the authors. Licensee MDPI, Basel, Switzerland. This article is an open access article distributed under the terms and conditions of the Creative Commons Attribution (CC BY) license (<https://creativecommons.org/licenses/by/4.0/>).

1. Introduction

Activation and utilization of carbon dioxide [1], a major greenhouse gas, has the potential to address two key contemporary environment related problems: global warming due to increasing CO₂ emission and provision of carbon-neutral energy [2]. Electrocatalytic conversion of carbon dioxide to carbon monoxide [3] is considered one of the viable options for CO₂ fixation [4], where liquid fuels [5] and other commodity chemicals can be made from the resulting carbon monoxide in combination with hydrogen gas using the Fischer–Tropsch technique [6].

Molecular organometallic electrocatalysts [7] for electroreduction of carbon dioxide [8] have been extensively reviewed [9], and trends within d-block metals have been elaborated [10–12]. Considering the need for ultimate scale-up of the catalytic process for CO₂ reduction, designing catalysts using earth abundant transition metals [13], such as Fe [14,15], Ni [16,17], and Co [18,19], has received significant interest. Manganese is one of the most Earth abundant transition metals [20], and has been shown to replace rhenium [21] in CO₂ reduction catalysts [22,23]. Hence, a wide-range of ligands have been attached to a manganese tricarbonyl halide core [24–26], including N-heterocyclic carbene [27,28], non-aromatic diamine [29], pincer ligands [30], and P-coordinating ligands [31]. There are a wide range of recent examples exploring structure-activity and mechanistic questions of these organomanganese electrocatalysts [32–39].

Thus, we began a study of aromatic diamine ligands, attached to either a manganese or rhenium tricarbonyl halide core. We report the novel compounds Mn(benzene-1,2-diamine)(CO)₃Br, **Mn-1**, Mn(3-methylbenzene-1,2-diamine)(CO)₃Br, **Mn-2**, and Re(benzene-1,2-diamine)(CO)₃Cl,

Re-1 (Figure 1). The historical compounds Mn(benzene-1,2-diamine)(CO)₄ [40] and Re(*o*-benzoquinone diimine)(CO)₃Cl [41] have each been reported on a single occasion, without any analysis for carbon dioxide electroreduction. In addition to synthesis and characterization, X-ray crystallography (**Mn-2** and **Re-1**), electrochemistry, and electrocatalytic studies for the reduction of CO₂ to CO by three novel organometallic diamine complexes are presented. The use of ligands bound to a metal via an amine group in successful organometallic electrocatalysts for carbon dioxide reduction is reported herein [42].

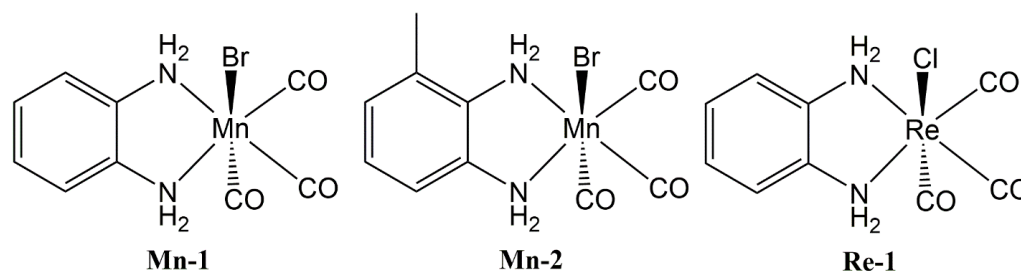
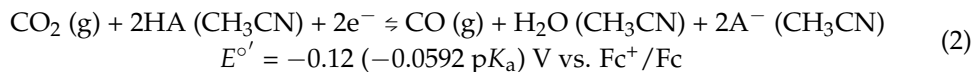


Figure 1. Structures of the novel organometallic complexes studied herein: Mn(benzene-1,2-diamine)(CO)₃Br, **Mn-1**, Mn(3-methylbenzene-1,2-diamine)(CO)₃Br, **Mn-2**, and Re(benzene-1,2-diamine)(CO)₃Cl, **Re-1**.

Electrochemistry will be utilized to determine turnover frequency (TOF) and overpotential from cyclic voltammetry (CV) of solutions of the compounds under an atmosphere of CO₂.

$$\text{TOF} = 0.1992 \left(\frac{Fv}{RT} \right) \left(\frac{n_p^3}{n_{cat}^2} \right) \left(\frac{i_{cat}}{i_p} \right)^2 \quad (1)$$



where i_{cat} is the peak current of the catalyzed reaction and n_{cat} is the number of electrons involved in that catalytic process, while i_p is the peak current of the compound under non-catalytic conditions and n_p is the number of electrons involved in that process. F is the Faraday constant, v is the applied scan rate, R is the universal gas constant, and T is the temperature in Kelvin. Subsequently, TOFs may be determined using Equation (1) [43].

Overpotential is also a useful metric for analysis of electrocatalysts, indicating how much additional potential is required beyond the thermodynamic amount for a given reaction. As we are exploring the reduction of carbon dioxide to carbon monoxide in the presence of a proton source, we will use Equation (2), where the thermodynamic potential is known to change with the strength of the acid chosen as the proton source [44].

2. Results and Discussion

2.1. Synthesis

Complexes **Mn-1** and **Mn-2** were synthesized by combining manganese pentacarbonyl bromide and the appropriate benzenediamine ligand in THF at reflux under an inert atmosphere. Complex **Re-1** was synthesized by combining rhenium pentacarbonyl chloride and benzene-1,2-diamine in toluene at reflux under an inert atmosphere. Metal pentacarbonyl halide to ligand ratios were 1:1 to avoid the formation of complex salts, such as [Re(benzene-1,2-diamine)₂(CO)₃]Br [45]. Upon removal of THF/toluene by rotary evaporation, resolution in minimal acetone was followed by crystallization from pentane, yielding dark green manganese compounds and a pale purple rhenium product.

2.2. Solid State Structure

Single crystals suitable for X-ray diffraction studies were grown via hexane vapor diffusion into a dichloromethane solution of **Mn-2**, and via slow evaporation of a diethyl ether solution of **Re-1**. Structures displayed tricarbonyl *fac* orientation (Figures 2 and 3),

with an average metal–carbon bond length of 1.79 Å for **Mn-2** and 1.91 Å for **Re-1**, and metal–halide bond lengths of 2.55 Å and 2.51 Å, respectively.

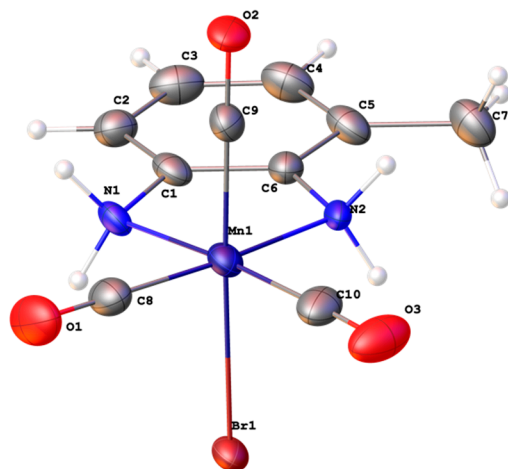


Figure 2. ORTEP diagram of **Mn-2** (30% probability thermal ellipsoids). The structure displays the presence of *fac*-[Mn(CO)₃] with coordinated diamine and bromide ligand.

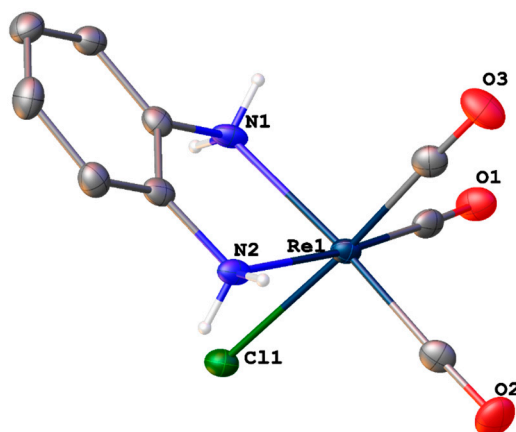


Figure 3. ORTEP diagram of **Re-1** (50% probability thermal ellipsoids). The structure displays the presence of *fac*-[Re(CO)₃] with coordinated diamine and chloride ligand.

2.3. Spectroscopy

UV/Visible absorption spectroscopy reveals similar MLCT bands for **Mn-1** and **Mn-2**, with a molar attenuation coefficient ~20% greater for **Mn-2** (Figure 4). Studies of tricarbonyl halide diimine compounds saw blue-shifts of 30–60 nm for replacement of Mn with Re [46]. Specifically with phenanthroline ligands, blue-shifts of ~45 nm are concomitant with a cathodic shift in reduction potential of ~250 mV [47]. As Re is switched to Mn herein, a cathodic shift in reduction potential of 450 mV is observed (Table 1), allowing a possible assignment of an MLCT to the absorption peak at 261 nm, a 98 nm blue shift (although IL π to π^* absorptions are common in this region). This **Re-1** putative MLCT has a molar attenuation coefficient of ~3-fold that of the manganese compounds, and is similar in magnitude to Re tricarbonyl halide diimines (~5000 M⁻¹ cm⁻¹) [48]. A weak absorption feature (88 M⁻¹ cm⁻¹) is seen for **Re-1**, occurring at ~180 nm red-shift compared to the MLCT of the manganese compounds (Figure 4, inset), which is likely a low probability MLCT [49], occurring at a wavelength very close to that seen for a much stronger MLCT seen in Re(o-benzoquinone diimine)(CO)₃Cl [50].

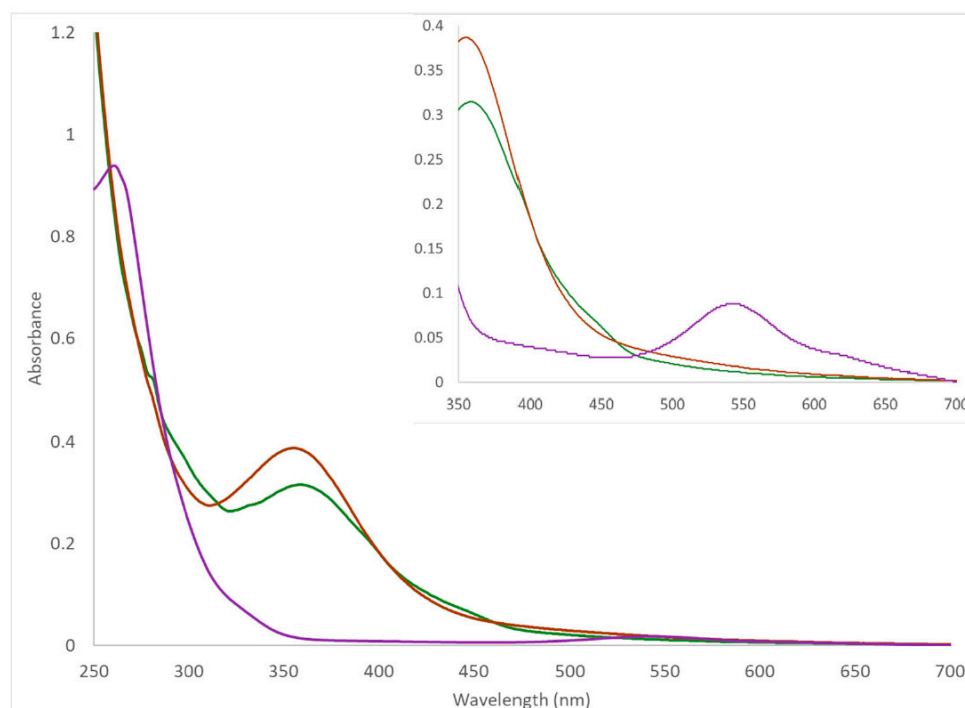


Figure 4. UV/Vis spectra of **Mn-1** (green), **Mn-2** (brown) and **Re-1** (purple), all 0.200 mM in acetonitrile. Inset: **Re-1** concentration increased to 1.00 mM in acetonitrile.

Table 1. Reduction/oxidation potentials, infrared and UV/Vis data for **Mn-1**, **Mn-2**, and **Re-1**. IR absorption peaks are attributed to CO stretching modes.

Complex	E_{pc1} (V) ^a	E_{pa1} (V) ^a	$\tilde{\nu}_{CO}$ (cm ⁻¹) ^b	Mean $\tilde{\nu}_{CO}$ (cm ⁻¹)	MLCT (nm) ^c	ϵ M ⁻¹ cm ⁻¹
Mn-1	−2.30	0.60	2028, 1931, 1890	1950	359	1580
Mn-2	−2.35	0.62	2030, 1932, 1888	1950	355	1930
Re-1	−2.75	0.89	2025, 1915, 1861	1934	261, 543	4700, 88

^a Potential at peak of first reduction/oxidation wave vs. Fc/Fc⁺ at 0.100 V s⁻¹ in 0.100 M *n*-Bu₄NPF₆ in anhydrous acetonitrile. ^b Recorded in solid state. ^c Recorded in acetonitrile.

IR spectroscopy of the carbonyl region displays three absorption peaks for all three compounds studied, displaying near identical wavenumbers for **Mn-1** and **Mn-2**, correlating well to near identical reduction and oxidation potentials. **Re-1** has a mean $\tilde{\nu}_{CO}$ some 16 cm⁻¹ lower than the manganese compounds, indicative of stronger carbonyl binding due to greater electron density upon the central metal (supported by the observation of a more cathodic reduction). IR spectroscopy also displays the expected N-H bond absorbances in the 3100–3300 cm⁻¹ region (Figures S9–S11), further supporting structural assignment.

NMR spectroscopy in acetone-d₆ also confirms structural assignment, most clearly in the large downfield shift and loss of symmetry of the amine protons, seen in a single broad peak at 3.98 ppm in free benzene-1,2-diamine. Upon attachment of the ligand to the metal, the amine protons are seen as two equal integration irregular peaks at 6.58 and 4.88 ppm in **Mn-1**, and 6.88 and 5.50 ppm in **Re-1** (Figures S12–S15). Attachment of 3-methylbenzene-1,2-diamine ligand (broad doublet at 3.87 ppm in free ligand) sees a similar shift upon attachment to manganese, yielding four equal integration irregular doublets at 6.58, 6.38, 4.88, and 4.67 ppm for **Mn-2** with approximate splitting constants of 5 to 10 Hz (Figure S14). ¹³C NMR of **Mn-2** (Figure S15) displays the anticipated 6 unique aromatic carbon atoms in the 140 to 127 ppm range, and a methyl carbon at 16.9 ppm (typically weak carbonyl carbon signals are obscured by the solvent).

The integration for the amine protons in **Mn-1** and **Re-1** is ~25% lower than anticipated, a feature that is preliminarily ascribed to exchangeability of these protons (the four amine proton peaks in the asymmetrical **Mn-2** have only ~5% lower integration than expected). While no additional peaks are visible, concerns have been raised that this observation indicates that the benzene-1,2-diamine ligand is attached in a diimine manner. HRMS displayed two major peaks of similar size, one corresponding to the loss of halide and addition of an acetonitrile molecule, the second corresponding to just loss of halide [51]. No peaks were observed corresponding to compounds containing an *o*-benzoquinone diimine. Rhenium was confirmed by HRMS as present in **Re-1** due to the observation of the predicted peak ratio due to the two primary rhenium isotopes. Elemental analysis also confirms the diamine molecular assignment of the three compounds studied herein. Table S1 details how alternative *o*-benzoquinone diimine compounds would not match the elemental analysis results for our compounds, lacking a match to the experimentally obtained values for hydrogen percentage. Additional evidence for diamine (rather diimine) ligands is seen in the bond lengths observed in the Xray crystallographic structures of **Mn-2** and **Re-1**, where C-N bond lengths are 1.45 to 1.47 Å, matching the 1.47 Å average seen in amines, and far from the 1.28 Å average seen in imines [52].

2.4. Photochemistry

Organomanganese carbonyl compounds have long been reported as unstable upon light exposure [53], such that we carried out all our reactions and analyses with our compound in foil-wrapped glassware. Acetonitrile solutions of our three compounds were tracked for decomposition by UV/Vis over 90 min of exposure to ambient lab lighting. While **Re-1** was unchanged, **Mn-1** had a small amount degradation, ~3% change at λ_{\max} of 359 nm, and a small feature grew in at ~770 nm beyond 60 min of exposure. **Mn-2** was more prone to decomposition, with ~5% change at λ_{\max} of 355 nm, and a degree of broadening of the main absorption feature (Figure S17).

Mn-1 and **Mn-2** both display fluorescence upon excitation at their λ_{\max} wavelengths, 359 and 355 nm, respectively (Figure S18). **Mn-1** emission is centered at 522 nm, while **Mn-2** emission is centered at 541 nm, indicating greater energy loss to relaxation prior to emission, perhaps due to the lower symmetry molecule having more vibrational modes. Both manganese compounds had a minor (~20% the intensity of the main peak) secondary peak at longer wavelengths of 715 and 710 nm, respectively. **Re-1** did not display any fluorescence upon excitation at either 261 or 543 nm.

2.5. Electrochemistry

All complexes exhibit a single irreversible reduction peak during cyclic voltammetry (CV), occurring at -2.30 V vs. Fc^+/Fc under an argon atmosphere for **Mn-1** (Figure S1), with the reduction potential of **Mn-2** being slightly (50 mV) more negative than **Mn-1** (Figure S2), indicative of a very modest increase in electron density, due to methylation upon the benzene ring [54] of the diamine. Support for this assignment can be found in the carbonyl group IR absorbance, where wavenumbers vary by just 2 cm^{-1} for the most labile CO. The reduction of **Re-1** occurs a further 300 mV more negative, indicating more challenging reduction, and suggestive of more electron density upon the Re atom (as also indicated by the IR spectra of the carbonyl groups). Reductions are irreversible at the scan rates studied, appearing to be two-electron processes (based upon exhaustive controlled potential electrolysis of the compounds) and are assigned to loss of the halide ligand and formation of an anion [55].

The oxidation potential of the manganese compounds are almost identical at ~ 0.6 V vs. Fc^+/Fc , while the oxidation of **Re-1** occurs almost 300 mV more positive (Figure S3). All oxidations are irreversible and show large currents (greater than one or two electron processes) indicative of compound decomposition.

2.6. Electrocatalysis

All complexes were studied in acetonitrile under an atmosphere of CO₂ in the presence of a proton source, trifluoroethanol (TFE). Addition of TFE to a solution of **Mn-1** yielded enhancement in current at ca. -2.5 V (Figure 5), broadly similar to the effect seen with **Mn-2** (Figure S4). The proposed catalytic mechanism (Scheme S1) suggests that initial reduction yields a catalyst that then cycles via a two electron two proton catalytic cycle, hence an enhancement of current is commonly interpreted as a catalytic process [8]. The reduction feature of **Mn-1** (and **Mn-2**) occur at the same potential under a CO₂ atmosphere; however, there is a change from a distinct peak under argon to a plateau under carbon dioxide, suggestive that the reduced complex binds substrate but no catalytic conversion occurs. This reduction feature is then seen to increase with increased concentration of TFE, an effect that is broadly absent in a similar study with **Re-1** (Figure S5), and completely absent in the catalyst-free control experiment (Figure S6).

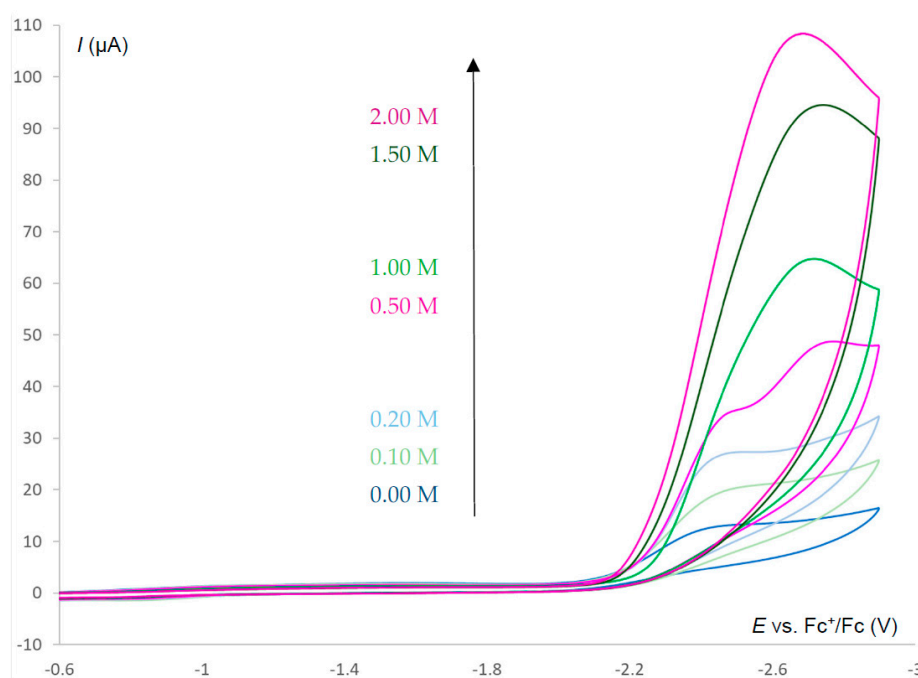


Figure 5. Cyclic voltammetry of 1.010 mM of **Mn-1** (blue) with subsequent additions of trifluoroethanol, TFE: 0.10 M, 0.20 M, 0.50 M, 1.00 M, 1.50 M, 2.00 M. Recorded in 0.100 M Bu_4NPF_6 in dry CO₂-saturated acetonitrile on a 3.00 mm diameter glassy carbon electrode vs. Fc^+/Fc at 0.100 V/s.

The addition of an external proton source to a solution of **Mn-1** yields an increase in current due to the electrocatalytic reduction of carbon dioxide to carbon monoxide (vide infra). Homogeneous organometallic CO₂ reduction electrocatalysts require either an internal proton source [56] or deliberate addition of an external proton source. The catalytically active species, obtained from electrochemical reduction, binds carbon dioxide but is unable to cleave one of the subsequent C-O bonds without the addition of a proton [57]. The catalytic current produced increases with increasing proton concentration (affected by either increased acid concentration or increased acid strength) [58]. A study of **Mn-2** under a CO₂ atmosphere with additions of water showed only a limited catalytic current (Figure S7); hence, our study focused upon the use of a stronger proton source, TFE. Additionally, a catalyst concentration study of **Mn-2** in the presence of a fixed concentration of TFE shows a near linear response to increasing catalyst concentration, indicating a first-order process (Figure 6), and that catalysis is dependent upon the presence of the organomanganese electrocatalyst. The transfer of the working electrode used in a CO₂/TFE study (with each manganese catalyst) into a catalyst-free solution containing CO₂ and TFE displayed no catalytic process, supportive of assignment of homogeneous catalysis.

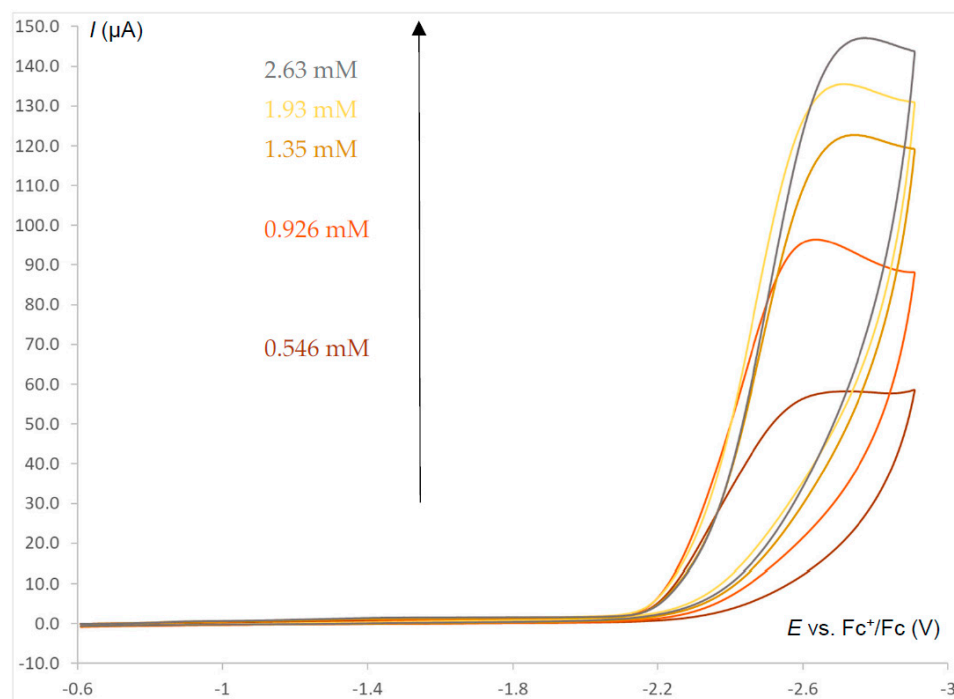


Figure 6. Cyclic voltammetry of indicated concentrations of **Mn-2** with 2.00 M trifluoroethanol. Recorded in 0.100 M Bu_4NPF_6 in dry CO_2 -saturated acetonitrile on a 3.00 mm diameter glassy carbon electrode vs. Fc^+/Fc at 0.100 V/s.

The i_{cat}/i_p can be determined from CV data in the acid-independent region of catalysis [59], where i_{cat} and i_p are the peak current of the catalyzed and non-catalyzed reactions, respectively. Entry into a true acid-independent region (by sufficient addition of acid to obtain a plateau in current) was not possible for our catalysts, due to solubility of the compounds becoming a problem at high values of added TFE. One solution to this problem would be to use less of a stronger (more acidic) proton source, although our concern preventing this was the competing reduction of the acid (or, rather, the carbonic acid that is made in situ) to hydrogen, due to our catalysts only being active at negative potentials where such competing reduction is an issue. However, the largest addition of TFE where no precipitation occurred (2.0 M) can be used as a proxy for the acid independent region by providing a reasonable minimum value for an i_{cat}/i_p , and hence a minimum value for a TOF for our catalysts.

The i_{cat}/i_p for **Mn-1** was 8.3 and for **Mn-2** it was 7.7 (Figure 7). These values may then be used in Equation (2) to find a turnover frequency (TOF) for the catalyst being studied [60], yielding values of 108 s^{-1} for **Mn-1** and 82 s^{-1} for **Mn-2**. CV of **Mn-1** vs. **Mn-2** under catalytic conditions (in the presence of proton source and CO_2) indicates that **Mn-1** is the better catalyst, with an i_{cat}/i_p value that is ~8% greater than for **Mn-2**. Given an electron donating methyl group on the ligand platform, **Mn-2** was expected to produce a higher catalytic current than that of **Mn-1** through a mild electronic effect that would enhance electron density upon the metal center and increase nucleophilic attacks upon the CO_2 (Scheme S1) [61]. This lack of improvement suggests that the binding of CO_2 by the catalyst is not rate-determining, but rather that the rate-determining step may be reductive cleavage of the Mn-CO (intermediate D to intermediate A, Scheme S1), a step that would be slower when metal center electron density is increased. With increased electron density on the metal, the Mn-CO bond would be stronger in **Mn-2** due to greater back-bonding from metal to ligand, as compared to the case of **Mn-1**. The TOF values for our manganese compounds are somewhat low compared with the majority of published systems, with catalysis occurring at a disappointingly negative potential [62]. However,

this initial example of diamine ligand use in carbon dioxide electrocatalyst design, as a proof of concept, could lead to exploration of the use of similar ligand platforms.

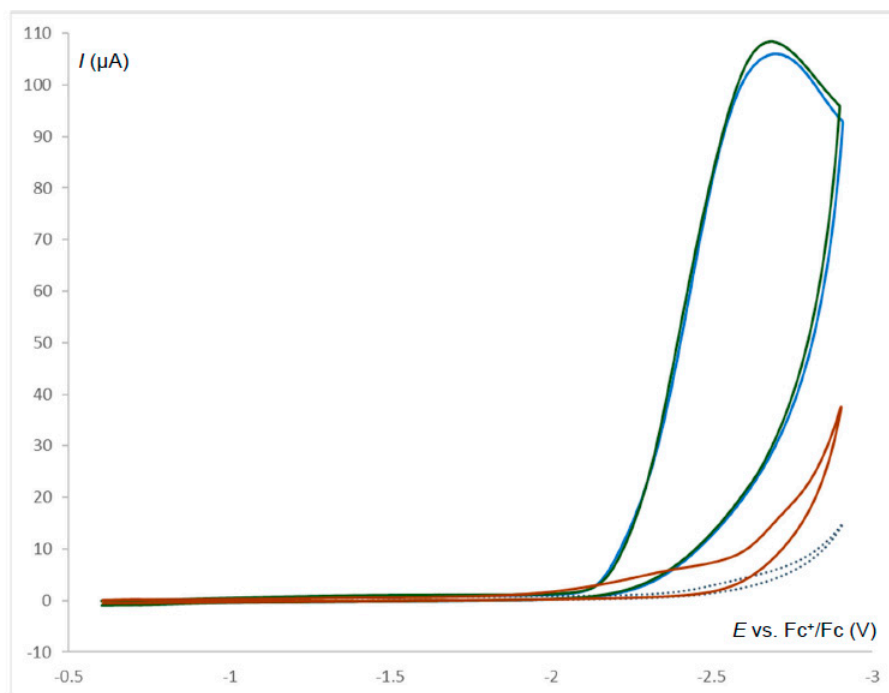


Figure 7. Cyclic voltammetry of 2.00 M TFE (dotted line); 2.00 M TFE + 1.010 mM of **Mn-1** (dark green); 2.00 M TFE + 1.002 mM of **Mn-2** (blue); 2.00 M TFE + 0.992 mM of **Re-1** (brown). Recorded in 0.100 M Bu_4NPF_6 in dry CO_2 -saturated acetonitrile on a 3.00 mm diameter glassy carbon electrode vs. Fc^+/Fc at 0.100 V/s.

Our use of a weak acid proton source, namely trifluoroethanol (TFE) allows us to use Equation (2), with an estimated pK_a of 35.4 for TFE [63], to arrive at a thermodynamic potential of -2.22 V. The potential at half peak height of the catalytic peak is used as a proxy for the $E_{1/2}$ in irreversible systems (which the catalytic peak represents); in our case, a value ca. -2.4 V is observed, which represents a relatively low overpotential of ca. 0.18 V.

The limited electrocatalysis observed with **Re-1** is consistent with examples where Re catalysts have TOF values around an order of magnitude lower than the analogous Mn compound [64]. In particular, in our case, **Re-1** appears to reduce at too negative a potential, such that should any Re-CO adduct be forming, its reduction potential lies too negative (at/beyond the solvent window). Given that there is only a small increase in current at the edge of our solvent window (Figure S5), it is not possible to obtain an accurate i_{cat}/i_p for **Re-1**, although it is likely <1.5 .

CV of solutions of each catalyst in acetonitrile under argon with 2.00 M TFE displayed no peak, indicating that there is no competing proton reduction directly of the TFE [65]. Additionally, a CV of an acetonitrile electrolyte solution containing the same increments of TFE additions and saturated with carbon dioxide displays only a minor response (Figure S6), indicative of a negligible direct electrode response [66].

Controlled Potential Electrolysis (CPE) was performed upon all three compounds, as well as upon “catalyst-free” control experiment conditions, with the electrocatalysis products being quantified by headspace Gas Chromatography (GC) [67]. Comparison to authentic samples of CO and H_2 (Figure S19) allowed the confirmation and quantification of the formation of carbon monoxide under these conditions with both manganese compounds. The performance of **Mn-1** and **Mn-2** are equivalent after electrolysis for 90 min, displaying faradaic yields of $\sim 85\%$ for CO production, with minimal co-production of H_2 (Table 2). An effective turnover of ~ 7.5 for the manganese catalysts, where turnover is moles product

divided by moles catalyst, establishes true catalysis with these manganese compounds, and given our 90 min CPE, equates to a turnover number (TON) of 5 h^{-1} . **Re-1** is inactive under the study conditions, producing ~2% the CO of the manganese compounds. CPE confirms the lack of activity of **Re-1** that is implied by our earlier CV analysis.

Table 2. CPE data for **Mn-1**, **Mn-2**, and **Re-1**, compared to catalyst-free conditions ^a.

	Q (C)	$\mu\text{mol CO}$	FE ^b CO (%)	$\mu\text{mol H}_2$	FE ^b H ₂ (%)
Mn-1	35 ± 1.4	157 ± 5	86 ± 3	2.9 ± 0.9	1.6 ± 0.8
Mn-2	33 ± 2	148 ± 6	85 ± 4	2.6 ± 0.7	1.5 ± 0.7
Re-1	2.2 ± 0.6	3.1 ± 0.5	27 ± 5	2.4 ± 0.4	21 ± 4
Catalyst-free	1.6 ± 0.4	0.6 ± 0.4	7 ± 4	5.4 ± 0.8	65 ± 10

^a 0.500 mM (20.0 μmol) of catalyst in each case, in 1.50 M TFE, 0.100 M Bu_4NPF_6 in dry CO_2 -saturated acetonitrile on a carbon rod electrode at -2.20 V vs. Fc/Fc^+ for 90 min (mean of three trials). ^b FE = Faradaic efficiency = charge to form product/total charge passed.

CPE was stopped after 90 min for convenience and a desire to not cause pressure leaks in our reaction vessel during electrolysis. The organomanganese compounds were still active at this 90 min time point. Currents drop to around 80% of their initial value within a few minutes of initiation of electrolysis, and are from then mostly stable, slowly dropping to around 70–75% by the 90 min mark. If catalysis had ceased, then current would drop to zero, as it almost does for **Re-1** and catalyst-free CPE. CV of the electrolysis solution upon completion of CPE still retains the catalytic peak, albeit somewhat diminished, to around 70% of the initial current value, indicative of some loss of organomanganese catalyst. An example FTIR spectra of a post electrolysis solution of **Mn-2** clearly displays a tricarbonyl pattern (Figure S11). The pattern has peaks that are $1\text{--}2 \text{ cm}^{-1}$ different from solid **Mn-2**, which could be an artefact of instrument precision or solvation, but does not preclude the formation of $\text{Mn}(\text{3-methylbenzene-1,2-diamine})(\text{CO})_3(\text{CH}_3\text{CN})$ [68].

3. Experiment/Characterization

Materials: All the reagents were used as received from the following: tetrabutylammonium hexafluorophosphate (Bu_4APF_6 , Sigma, St. Louis, MI, USA), anhydrous acetonitrile (Sigma), manganese pentacarbonyl bromide ($\text{Mn}(\text{CO})_5\text{Br}$, Strem), rhenium pentacarbonyl chloride ($\text{Re}(\text{CO})_5\text{Cl}$, Sigma), benzene-1,2-diamine (TCI), 3-methylbenzene-1,2-diamine (Acros Organics).

Synthesis: All reactions were carried out in an inert atmosphere of argon using standard Schlenk techniques. All reactions involving manganese complexes were protected from light during reaction, storage and electrochemistry (using aluminum foil wrap).

Mn(benzene-1,2-diamine)(CO)₃Br (Mn-1**):** $\text{Mn}(\text{CO})_5\text{Br}$ (0.2020 g, 0.733 mmol) and 1,2-phenylenediamine (0.0800 g, 0.740 mmol) were combined in tetrahydrofuran (30 mL), and the mixture was purged in argon for 10 min before being stirred at reflux for one hour. A color change occurred during reflux, changing from the faint orange to black/green. The tetrahydrofuran was removed by use of a rotary evaporator until dryness, and acetone (2 mL) and pentane (50 mL) were added, forming a green precipitate. The product was cooled in an isothermometer freezer ($-20 \text{ }^\circ\text{C}$) and then filtered and rinsed with pentane. The final green solid was dried under reduced pressure for approximately 24 h, obtaining an 76% yield. IR (solid, $\tilde{\nu}_{\text{CO}}$): 2028 cm^{-1} , 1931 cm^{-1} , 1890 cm^{-1} . MS (m/z): calc: 246.9915, found: 246.9913 (M-Br^+), calc: 288.0181, found: 288.0176 (M-Br+MeCN^+). UV/Vis in MeCN (ϵ , $\text{M}^{-1} \text{ cm}^{-1}$): 359 nm (1580). ¹H NMR (300 MHz, $(\text{CD}_3)_2\text{CO}$, ppm) δ : 7.49 (2H, s), 7.30 (2H, s), 6.58 (2H, m), 4.88 (2H, m). Anal. Calc. for $\text{C}_9\text{H}_8\text{BrN}_2\text{O}_3\text{Mn}$: C, 33.06; H, 2.47; N, 8.57. Anal. Found: C, 33.34; H, 2.65; N, 8.42.

Mn(3-methylbenzene-1,2-diamine)(CO)₃Br (Mn-2**):** $\text{Mn}(\text{CO})_5\text{Br}$ (0.2010 g, 0.730 mmol) and 2,3-diaminotoluene (0.0901 g, 0.738 mmol) were combined in tetrahydrofuran (30 mL), and the mixture was purged with argon for ten minutes before stirring at reflux for one hour.

A color change occurred during reflux from pale orange to dark green. The tetrahydrofuran was removed by rotary evaporator until dryness, and acetone (2 mL) and pentane (50 mL) were added, forming a brown/green precipitate. The product was cooled in an isotemp freezer ($-20\text{ }^{\circ}\text{C}$) and then filtered and rinsed with pentane. The final brown/green solid was dried under reduced pressure for approximately 24 h, obtaining an 86% yield. IR (solid, $\tilde{\nu}_{\text{CO}}$): 2030 cm^{-1} , 1932 cm^{-1} , 1888 cm^{-1} . MS (m/z): calc: 261.0071, found: 261.0064 (M-Br)⁺, calc: 302.0337, found: 302.0334 (M-Br+MeCN)⁺. UV/Vis in MeCN (ϵ , $\text{M}^{-1}\text{ cm}^{-1}$): 355 nm (1930). ¹H NMR (300 MHz, $(\text{CD}_3)_2\text{CO}$, ppm) δ : 7.32 (1H, m), 7.18 (2H, m), 6.58 (1H, d, 5.1 Hz), 6.38 (1H, d, 10.5 Hz) 4.88 (1H, d, 9 Hz), 4.67 (1H, d, 9.3 Hz), 2.54 (3H, s). ¹³C NMR (75 MHz, $(\text{CD}_3)_2\text{CO}$, ppm) δ : 139.7, 138.2, 135.6, 128.4, 126.9, 124.2, 16.9 (carbonyl C obscured by solvent). Anal. Calc. for $\text{C}_{10}\text{H}_{10}\text{BrMnN}_2\text{O}_3$: C, 35.22; H, 2.96; N, 8.21. Anal. Found: C, 35.50; H, 2.94; N, 8.06. Crystals suitable for X-ray diffraction were obtained by vapor diffusion of hexane into a solution of the complex in dichloromethane at $-20\text{ }^{\circ}\text{C}$, CCDC 1893661.

Re(benzene-1,2-diamine)(CO)₃Cl (**Re-1**): Re(CO)₅Cl (0.2002 g, 0.553 mmol) and 1,2-phenylenediamine (0.0607 g, 0.562 mmol) were combined in toluene (50 mL) and the mixture was purged with argon for 10 min before being stirred at reflux for two hours. A color change occurred during reflux, changing from uncolored to purple. The toluene was removed by use of a rotary evaporator until dryness, and acetone (2 mL) and pentane (50 mL) were added, forming a pale purple precipitate. The product was cooled in an isothermperature freezer ($-20\text{ }^{\circ}\text{C}$), and then filtered and rinsed with pentane. The final solid was dried under reduced pressure for approximately 24 h, obtaining an 80% yield. IR (solid, $\tilde{\nu}_{\text{CO}}$): 2025 cm^{-1} , 1915 cm^{-1} , 1861 cm^{-1} . UV/Vis in MeCN (ϵ , $\text{M}^{-1}\text{ cm}^{-1}$): 261 nm (4700), 543 nm (88). ¹H NMR (400 MHz, $(\text{CD}_3)_2\text{CO}$, ppm) δ : 7.50 (2H, m), 7.31 (2H, m), 6.88 (2H, d), 5.50 (2H, d). MS (m/z): calc: 379.0093, found: 379.0106 (M-Cl)⁺, calc: 420.0358, found: 420.0365 (M-Cl+MeCN)⁺. Anal. Calc. for $\text{C}_9\text{H}_8\text{ClN}_2\text{O}_3\text{Re}$: C, 26.12; H, 1.95; N, 6.77. Anal. Found: C, 26.37; H, 1.88; N, 6.82. Crystals suitable for X-ray diffraction were obtained by evaporation of diethyl ether solution of the complex at $-20\text{ }^{\circ}\text{C}$, CCDC 1893660.

Electrochemistry: All cyclic voltammograms (CVs) were obtained by using a CHI Model 600E Potentiostat 3-electrode cell with a glassy carbon 3 mm diameter working electrode, platinum wire counter electrode, and silver external reference electrode (10 mM AgNO₃ in electrolyte solution). The electrolyte solution for all experiments was 0.10 M tetra-n-butylammonium hexafluorophosphate (Bu₄NPF₆) in anhydrous acetonitrile (Aldrich). The potentials (E) at the working electrode in all CV's are reported with respect to the ferrocenium/ferrocene couple in electrolyte solution. The ferrocenium/ferrocene couple data was collected daily at the end of each experiment, confirming potential and that appropriate resistance compensation had been applied. All CVs reported are background corrected, i.e., the scan with only electrolyte present was subtracted from the raw data. All background scans confirmed the sufficient removal of O₂ as seen (Figure S20) by the absence of a reduction peak ca. -1.2 V [69]. CVs were collected under the flow of ultra-high purity argon or bone-dry carbon dioxide gases. Controlled Potential Electrolysis (CPE) experiments were performed using a two-compartment cell: one compartment containing a carbon rod working electrode (effective surface area = 5.5 cm^2) and an Ag/AgNO₃ pseudo-reference electrode, the other compartment containing a carbon rod counter electrode (effective surface area = 8.0 cm^2). Head-space gas was tested after 90 min of electrolysis.

Instrumentation: NMR spectra were recorded on a 300 or 400 MHz Bruker NMR spectrometer. Mass spectra were recorded on an Agilent 6500 Series Q-TOF LC/MS in acetonitrile solution. Electronic absorption spectra were recorded on a Shimadzu UV-2600 UV-visible spectrometer. FTIR data was obtained using a Perkin Elmer 100 spectrometer, at 1.0 cm^{-1} resolution. Elemental analysis was carried out by Atlantic Microlabs (Norcross, GA, USA).

4. Conclusions

Two new earth abundant metal-based catalysts, Mn(benzene-1,2-diamine)(CO)₃Br (**Mn-1**) and Mn(3-methylbenzene-1,2-diamine)(CO)₃Br (**Mn-2**) have been synthesized and characterized, which rapidly catalyze the reduction of carbon dioxide to carbon monoxide at low overpotential. The novel Re congener Re(benzene-1,2-diamine)(CO)₃Cl (**Re-1**) has been synthesized and characterized, but lacks such electrocatalytic activity. The reduction of **Re-1** occurs 0.40 V more cathodic than the manganese complexes, likely indicating that if **Re-1** were to undergo a similar mechanism, a catalytic peak further cathodic than the one seen for the manganese compounds would occur. We would likely not be able to see such a process due to competing direct reduction and the cathodic limit of the solvent window. [23,70] Use of diamine ligands could lead to an expansion of ligand options for organomanganese carbon dioxide reduction electrocatalysts.

Supplementary Materials: The following supporting information can be downloaded at: <https://www.mdpi.com/article/10.3390/inorganics11090374/s1>, References [71–73] cited in Supplementary Materials.

Author Contributions: Conceptualization, B.D. and G.A.N.F.; methodology, B.D., B.A.C. and A.S.P.; validation, J.G.S. and E.A.F.; formal analysis, G.A.N.F.; investigation, B.D., B.A.C., A.S.P., A.J.G. and G.A.N.F.; data curation, L.T.M.; writing—original draft preparation, B.D. and G.A.N.F.; writing—review and editing G.A.N.F.; supervision, G.A.N.F.; project administration, G.A.N.F.; funding acquisition, G.A.N.F. and G.S.N. collected and solved single crystal XRD data. All authors have read and agreed to the published version of the manuscript.

Funding: This research was funded by the Florida Space Grant Consortium.

Data Availability Statement: The data presented in this study are available within the article and supplementary material.

Acknowledgments: The authors gratefully acknowledge funding from the Florida Space Grant Consortium.

Conflicts of Interest: The authors declare no competing financial interest.

References

1. Sick, V. Spiers memorial lecture: CO₂ utilization: Why, why now, and how? *Faraday Discuss.* **2021**, *230*, 9–29. [CrossRef]
2. Appel, A.M.; Bercaw, J.E.; Bocarsly, A.B.; Dobbek, H.; DuBois, H.D.L.; Dupuis, M.; Ferry, J.G.; Fujita, E.; Hille, R.; Kenis, P.J.; et al. Frontiers, opportunities, and challenges in biochemical and chemical catalysis of CO₂ fixation. *Chem. Rev.* **2013**, *113*, 6621–6658. [CrossRef] [PubMed]
3. Lim, R.J.; Xie, M.; Sk, M.A.; Lee, J.; Fisher, A.; Wang, X.; Lim, K.H. A review on the electrochemical reduction of CO₂ in fuel cells, metal electrodes and molecular catalysts. *Catal. Today* **2014**, *233*, 169–180. [CrossRef]
4. DuBois, D.L. Development of molecular electrocatalysts for energy storage. *Inorg. Chem.* **2014**, *53*, 3935–3960. [CrossRef] [PubMed]
5. Benson, E.E.; Kubiak, C.P.; Sathrum, A.J.; Smieja, J.M. Electrocatalytic and homogeneous approaches to conversion of CO₂ to liquid fuels. *Chem. Soc. Rev.* **2009**, *38*, 89–99. [CrossRef] [PubMed]
6. Underwood, A. Industrial synthesis of hydrocarbons from hydrogen and carbon monoxide. *Ind. Eng. Chem.* **1940**, *32*, 449–454. [CrossRef]
7. Kinzel, N.W.; Werle, C.; Leitner, W. Transition metal complexes as catalysts for the electroconversion of CO₂: An organometallic perspective. *Angew. Chem. Int. Ed.* **2021**, *60*, 11628–11686. [CrossRef]
8. Costentin, C.; Robert, M.; Saveant, J. Catalysis of the electrochemical reduction of carbon dioxide. *Chem. Soc. Rev.* **2013**, *42*, 2423–2436. [CrossRef]
9. Francke, R.; Schille, B.; Roemelt, M. Homogeneously catalyzed electroreduction of carbon dioxide—Methods, mechanisms, and catalysts. *Chem. Rev.* **2018**, *118*, 4631–4701. [CrossRef]
10. Changcheng, C.; Nichola, A.W.; Machan, C.W. A look at periodic trends in d-block molecular electrocatalysts for CO₂ reduction. *Dalton Trans.* **2019**, *48*, 9454–9468. [CrossRef]
11. Grice, K.A. Carbon dioxide reduction with homogenous early transition metal complexes: Opportunities and challenges for developing CO₂ catalysis. *Coord. Chem. Rev.* **2017**, *336*, 78–95. [CrossRef]
12. Dalle, K.E.; Warnan, J.; Leung, J.J.; Reuillard, B.; Karmel, I.S.E. Reisner Electro- and solar-driven fuel synthesis with first row transition metal complexes. *Chem. Rev.* **2019**, *119*, 2752–2875. [CrossRef] [PubMed]
13. Fisher, B.J.; Eisenberg, R. Electrocatalytic reduction of carbon dioxide by using macrocycles of nickel and cobalt. *J. Am. Chem. Soc.* **1980**, *102*, 7361–7363. [CrossRef]

14. Costentin, C.; Drouet, S.; Robert, M.; Saveant, J. A local proton source enhances CO₂ electroreduction to CO by a molecular Fe catalyst. *Science* **2012**, *338*, 90–94. [[CrossRef](#)]
15. Oberem, E.; Roesel, A.F.; Rosas-Hernaandez, A.; Kull, T.; Fischer, S.; Spannenberg, A.; Junge, H.; Beller, M.; Ludwig, R.; Roemelt, M.; et al. Mechanistic insights into the electrochemical reduction of CO₂ catalyzed by iron cyclopentadienone complexes. *Organometallics* **2019**, *38*, 1236–1247. [[CrossRef](#)]
16. Froehlich, J.D.; Kubiak, C.P. Homogeneous CO₂ reduction by Ni(cyclam) at a glassy carbon electrode. *Inorg. Chem.* **2012**, *51*, 3932–3934. [[CrossRef](#)]
17. Mash, B.L.; Raghavan, A.; Ren, T. Ni^{II} complexes of C-substituted cyclam as efficient catalysts for reduction of CO₂ to CO. *Eur. J. Inorg. Chem.* **2019**, *2019*, 2065–2070. [[CrossRef](#)]
18. Lacy, D.C.; McCrory, C.C.L.; Peters, J.C. Studies of cobalt-mediated electrocatalytic CO₂ reduction using a redox-active ligand. *Inorg. Chem.* **2014**, *53*, 4980–4988. [[CrossRef](#)]
19. Chapovetsky, A.; Do, T.H.; Haiges, R.; Takase, M.K.; Marinescu, S.C. Proton-assisted reduction of CO₂ by cobalt aminopyridine macrocycles. *J. Am. Chem. Soc.* **2016**, *138*, 5765–5768. [[CrossRef](#)]
20. Valyaev, D.A.; Lavigne, G.; Lugan, N. Manganese organometallic compounds in homogeneous catalysis: Past, present, and prospects. *Coord. Chem. Rev.* **2016**, *308*, 191–235. [[CrossRef](#)]
21. Hawecker, J.; Lehn, J.; Ziessel, R.R. Photochemical and electrochemical reduction of carbon dioxide to carbon monoxide mediated by (2,2'-Bipyridine)tricarbonylchlororhenium(I) and related complexes as homogeneous catalysts. *Helv. Chim. Acta* **1986**, *69*, 1990–2012. [[CrossRef](#)]
22. Bourrez, M.; Molton, F.; Chardon-Noblat, S.; Deronzier, A. [Mn(bipyridyl)(CO)₃Br]: An abundant metal carbonyl complex as efficient electrocatalyst for CO₂ reduction. *Angew. Chem. Int. Ed.* **2011**, *50*, 9903–9906. [[CrossRef](#)] [[PubMed](#)]
23. Smieja, J.M.; Sampson, M.D.; Grice, K.A.; Benson, E.E.; Froehlich, J.D.; Kubiak, C.P. Manganese as a substitute for rhenium in CO₂ reduction catalysts: The Importance of acids. *Inorg. Chem.* **2013**, *52*, 2484–2491. [[CrossRef](#)] [[PubMed](#)]
24. Grills, D.C.; Ertem, M.Z.; McKinnon, M.; Ngo, K.T.; Rochford, J. Mechanistic aspects of CO₂ reduction catalysis with manganese-based molecular catalysts. *Coord. Chem. Rev.* **2018**, *374*, 173–217. [[CrossRef](#)]
25. Sinopoli, Porte, N.T.L.; Martinez, J.F.; Wasielewski, M.R.; Sohail, M. Manganese carbonyl complexes for CO₂ reduction. *Coord. Chem. Rev.* **2018**, *365*, 60–74. [[CrossRef](#)]
26. Stanbury, M.; Compain, J.-D.; Chardon-Noblat, S. Electro and photoreduction of CO₂ driven by manganese-carbonyl molecular catalysts. *Coord. Chem. Rev.* **2018**, *361*, 120–137. [[CrossRef](#)]
27. Agarwal, J.; Shaw, T.W.; Stanton, C.J.; Majetich, G.F.; Bocarsly, A.B.; Schaefer, H.F. NHC-Containing manganese(I) electrocatalysts for the two-electron reduction of CO₂. *Angew. Chem. Int. Ed.* **2014**, *53*, 5152–5155. [[CrossRef](#)]
28. Friães, S.; Realista, S.; Mourão, H.; Royo, B. N-Heterocyclic and mesoionic carbenes of manganese and rhenium in catalysis. *Eur. J. Inorg. Chem.* **2022**, *2022*, e202100884. [[CrossRef](#)]
29. Zeng, Q.; Tory, J.; Hartl, F. Electrocatalytic reduction of carbon dioxide with a manganese(I) tricarbonyl complex containing a nonaromatic alpha-diimine ligand. *Organometallics* **2014**, *33*, 5002–5008. [[CrossRef](#)]
30. Petersen, H.A.; Myren, T.H.T.; Luca, O.R. Redox-active manganese pincers for electrocatalytic CO₂ reduction. *Inorganics* **2020**, *8*, 62. [[CrossRef](#)]
31. Rao, G.K.; Pell, W.; Korobkova, I.; Richeson, D. Electrocatalytic reduction of CO₂ using Mn complexes with unconventional coordination environments. *Chem. Commun.* **2016**, *52*, 8010–8013. [[CrossRef](#)] [[PubMed](#)]
32. Siritanaratkul, B.; Eagle, C.; Cowan, A.J. Manganese carbonyl complexes as selective electrocatalysts for CO₂ reduction in water and organic solvents. *Acc. Chem. Res.* **2022**, *55*, 955–965. [[CrossRef](#)] [[PubMed](#)]
33. Scherpf, T.; Carr, C.R.; Donnelly, L.J.; Durawski, Z.S.; Gelfand, B.S.; Piers, W.E. A mesoionic carbene–pyridine bidentate ligand that improves stability in electrocatalytic CO₂ reduction by a molecular manganese catalyst. *Inorg. Chem.* **2022**, *61*, 13644–13656. [[CrossRef](#)] [[PubMed](#)]
34. Hong, W.; Luthra, M.; Jakobsen, J.B.; Madsen, M.R.; Castro, A.C.; Hammershøj, H.C.D.; Pedersen, S.U.; Balcells, D.; Skrydstrup, T.; Daasbjerg, K.; et al. Exploring the parameters controlling product selectivity in electrochemical CO₂ reduction in competition with hydrogen evolution employing manganese bipyridine complexes. *ACS Catal.* **2023**, *13*, 3109–3119. [[CrossRef](#)]
35. Singh, K.K.; Gerke, C.S.; Saund, S.S.; Zito, A.M.; Siegler, M.A.; Thoi, V.S. CO₂ activation with manganese tricarbonyl complexes by an H-atom responsive benzimidazole ligand. *Eur. J. Inorg. Chem.* **2023**, e202300796. [[CrossRef](#)]
36. Cohen, K.Y.; Evans, R.; Bocarsly, A.B. Extending the π-system in MnI diimine tricarbonyl complexes: Impacts on photochemistry, electrochemistry, and CO₂ catalytic reduction activity. *Eur. J. Inorg. Chem.* **2023**, e202300435. [[CrossRef](#)]
37. Florian, J.; Cole, J.M. Analyzing structure–Activity variations for Mn–carbonyl complexes in the reduction of CO₂ to CO. *Inorg. Chem.* **2023**, *62*, 318–335. [[CrossRef](#)]
38. Fernandez, S.; Franco, F.; Belmonte, M.M.; Friães, S.; Royo, B.; Luis, J.M.; Lloret-Fillol, J. Decoding the CO₂ reduction mechanism of a highly active organometallic manganese electrocatalysts: Direct observation of a hydride intermediate and its implications. *ACS Catal.* **2023**, *13*, 10375–10385. [[CrossRef](#)]
39. Eagle, C.; Neri, G.; Piercy, V.L.; Younis, K.; Siritanaratkul, B.; Cowan, A.J. A manganese complex on a gas diffusion electrode for selective CO₂ to CO reduction. *Sustain. Energy Fuels* **2023**, *7*, 2301–2307. [[CrossRef](#)]
40. Hieber, W.; Beck, W.; Zietler, G. Neuere anschauungen über reaktionsweisen der metallcarbonyle, insbesondere des mangancarbonyls. *Angew. Chem.* **1961**, *73*, 364–368. [[CrossRef](#)]

41. Knor, G.; Leirer, M.; Synthesis, A.V. characterization and spectroscopic properties of 1,2-diiminetricarbonylrhenium(I)chloride complexes with o-benzoquinone diimines as ligands. *J. Organomet. Chem.* **2000**, *610*, 16–19. [[CrossRef](#)]
42. Gonell, S.; Miller, A.J.M. Carbon dioxide electroreduction catalyzed by organometallic complexes. *Adv. Organomet. Chem.* **2018**, *70*, 1–69. [[CrossRef](#)]
43. McKinnon, M.; Belkina, V.; Ngo, K.T.; Ertem, M.Z.; Grills, D.C.J. Rochford An investigation of electrocatalytic CO₂ reduction using a manganese tricarbonyl biquinoline complex. *Front. Chem.* **2019**, *7*, 628. [[CrossRef](#)]
44. Stratakes, B.M.; Dempsey, J.L.; Miller, A.J.M. Determining the overpotential of electrochemical fuel synthesis mediated by molecular catalysts: Recommended practices, standard reduction potentials, and challenges. *ChemElectroChem* **2021**, *8*, 4161–4180. [[CrossRef](#)]
45. Gerber, T.I.A.; Betz, R.; Booyesen, I.N.; Potgieter, K.; Mayer, P. Coordination of bidentate aniline derivatives to the fac-[Re(CO)₃]⁺ core. *Polyhedron* **2011**, *30*, 1739–1745. [[CrossRef](#)]
46. Kottelat, E.; Lucarini, F.; Crochet, A.; Ruggi, A.; Zobi, F. Correlation of MLCTs of group 7 fac-[M(CO)₃]⁺ complexes (M = Mn, Re) with bipyridine, pyridinylpyrazine, azopyridine, and pyridin-2-ylmethanimine type ligands for rational photoCORM design. *Eur. J. Inorg. Chem.* **2019**, *2019*, 3758–3768. [[CrossRef](#)]
47. Kurtz, D.A.; Dhakal, B.; Hulme, R.J.; Nichol, G.S.; Felton, G.A.N. Correlations between photophysical and electrochemical properties for a series of new Mn carbonyl complexes containing substituted phenanthroline ligands. *Inorg. Chim Acta* **2015**, *427*, 22–26. [[CrossRef](#)]
48. Kurtz, D.A.; Dhakal, B.; Donovan, E.S.; Nichol, G.S.; Felton, G.A.N. Non-photochemical synthesis of Re (diimine)(CO)₂(L)Cl (L = phosphine or phosphite) compounds. *Inorg. Chem. Commun.* **2015**, *59*, 80–83. [[CrossRef](#)]
49. Kurtz, D.A.; Brereton, K.R.; Ruoff, K.P.; Tang, H.M.; Felton, G.A.N.; Miller, A.J.M.; Dempsey, J.L. Bathochromic shifts in rhenium carbonyl dyes induced through destabilization of occupied orbitals. *Inorg. Chem.* **2018**, *57*, 5389–5399. [[CrossRef](#)]
50. Kunkely, H.; Vogler, A. Absorption spectra and CT transitions of compounds containing Re^I(CO)₃Cl, S²⁺ and Se²⁺ as donors and o-benzoquinone diimine as acceptor. *Inorg. Chem. Commun.* **2007**, *10*, 1236–1238. [[CrossRef](#)]
51. McIndoe, J.S.; Vikse, K.L. Assigning the ESI mass spectra of organometallic and coordination compounds. *J. Mass Spectrom.* **2019**, *54*, 466–479. [[CrossRef](#)] [[PubMed](#)]
52. Allen, F.H.; Kennard, O.; Watson, D.G.; Brammer, L.; Orpen, A.G.; Taylor, R. Tables of bond lengths determined by X-ray and neutron diffraction. Part 1. Bond lengths in organic compounds. *J. Chem. Soc. Perkin Trans. II* **1987**, *2*, S1–S19. [[CrossRef](#)]
53. Kottelat, E.; Fabio, Z. Visible Light-activated PhotoCORMs. *Inorganics* **2017**, *5*, 24. [[CrossRef](#)]
54. Donovan, E.S.; McCormick, J.J.; Nichol, G.S.; Felton, G.A.N. Cyclic voltammetric studies of chlorine-substituted benzenedithiolato-diiron hexacarbonyl electrocatalysts inspired by the [FeFe]-hydrogenase active site. *Organometallics* **2012**, *31*, 8067–8070. [[CrossRef](#)]
55. Kurtz, D.A.; Dhakal, B.; McDonald, L.T.; Nichol, G.S.; Felton, G.A.N. Inter-ligand intramolecular through-space anisotropic shielding in a series of manganese carbonyl phosphorous compounds. *Dalton Trans.* **2019**, *48*, 14296–14935. [[CrossRef](#)] [[PubMed](#)]
56. Franco, F.; Cometto, C.; Vallana, F.F.; Sordello, F.; Priola, E.; Minero, C.; Nervi, C.; Gobetto, R. A local proton source in a [Mn(bpy-R)(CO)₃Br]-type redox catalyst enables CO₂ reduction even in the absence of Brønsted acids. *Chem. Commun.* **2014**, *50*, 14670–14673. [[CrossRef](#)] [[PubMed](#)]
57. Wong, K.; Chung, W.; Lau, C. The effect of weak Brønsted acids on the electrocatalytic reduction of carbon dioxide by a rhenium tricarbonyl bipyridyl complex. *J. Electroanal. Chem.* **1998**, *453*, 161–170. [[CrossRef](#)]
58. Riplinger, C.; Carter, E.A. Influence of weak Brønsted acids on electrocatalytic CO₂ reduction by manganese and rhenium bipyridine catalysts. *ACS Catal.* **2015**, *5*, 900–908. [[CrossRef](#)]
59. Rountree, E.S.; McCarthy, B.D.; Eisenhart, T.T.; Dempsey, J.L. Evaluation of homogeneous electrocatalysts by cyclic voltammetry. *Inorg. Chem.* **2014**, *53*, 9983–10002. [[CrossRef](#)]
60. Tezuka, M.; Iwasaki, M. Voltammetric Study on CO₂ reduction electrocatalyzed by cobalt tetraphenylporphyrin in DMF solution. *Chem. Lett.* **1993**, *22*, 427–430. [[CrossRef](#)]
61. Bourrez, M.; Orio, M.; Molton, F.; Vezin, H.; Duboc, C.; Deronzier, A.; Chardon-Noblat, S. Pulsed-EPR evidence of a manganese(II) hydroxycarbonyl intermediate in the electrocatalytic reduction of carbon dioxide by a manganese bipyridyl derivative. *Angew. Chem. Int. Ed.* **2014**, *53*, 240–243. [[CrossRef](#)] [[PubMed](#)]
62. Nie, W.; McCrory, C.C.L. Strategies for breaking molecular scaling relationships for the electrochemical CO₂ reduction reaction. *Dalton Trans.* **2022**, *51*, 6993–7010. [[CrossRef](#)] [[PubMed](#)]
63. Lam, Y.Y.; Nielsen, R.J.; Gray, H.B.; Goddard, W.A. A Mn bipyrimidine catalyst predicted to reduce CO₂ at lower overpotential. *ACS Catal.* **2015**, *5*, 2521–2528. [[CrossRef](#)]
64. Barrett, J.A.; Miller, C.J.; Kubiak, C.P. Electrochemical reduction of CO₂ using group VII metal catalysts. *Trends Chem.* **2021**, *3*, 176–187. [[CrossRef](#)]
65. Felton, G.A.N.; Glass, R.S.; Lichtenberger, D.L.; Evans, D.H. Iron-only hydrogenase mimics. Thermodynamic aspects of the use of electrochemistry to evaluate catalytic efficiency for hydrogen generation. *Inorg. Chem.* **2006**, *45*, 9181–9184. [[CrossRef](#)]
66. McCarthy, B.D.; Martin, D.J.; Rountree, E.S.; Ullman, A.C.; Dempsey, J.L. Electrochemical reduction of Brønsted acids by glassy carbon in acetonitrile: Implications for electrocatalytic hydrogen evolution. *Inorg. Chem.* **2014**, *53*, 8350–8361. [[CrossRef](#)]
67. Cook, T.D.; Tyler, S.F.; McGuire, C.M.; Zeller, M.; Fanwick, P.E.; Evans, D.H.; Peters, D.G.; Ren, T. Nickel complexes of C-substituted cyclams and their activity for CO₂ and H⁺ reduction. *ACS Omega* **2017**, *2*, 3966–3976. [[CrossRef](#)]

68. Cohen, K.Y.; Nedd, D.G.; Evans, R.; Bocarsly, A.B. Mechanistic insights into CO₂ conversion to CO using cyano manganese complexes. *Dalton Trans.* **2023**, *52*, 7524–7537. [[CrossRef](#)]
69. Donovan, E.S.; Felton, G.A.N. Electrochemical analysis of cyclopentadienylmetal carbonyl dimer complexes: Insight into the design of hydrogen-producing electrocatalysts. *J. Organomet. Chem.* **2011**, *711*, 25–34. [[CrossRef](#)]
70. Mukherjee, J.; Siewert, I. Manganese and rhenium tricarbonyl complexes equipped with proton relays in the electrochemical CO₂ reduction reaction. *Eur. J. Inorg. Chem.* **2020**, e202000738. [[CrossRef](#)]
71. Dolomanov, O.V.; Bourhis, L.J.; Gildea, R.J.; Howard, J.A.K.; Puschmann, H. Olex2: A complete structure solution, refinement and analysis program. *J. Appl. Cryst.* **2009**, *42*, 339–341. [[CrossRef](#)]
72. Sheldrick, G.M. A short history of ShelX. *Acta Cryst.* **2008**, *A64*, 339–341.
73. Sheldrick, G.M. Crystal structure refinement with ShelXL. *Acta Cryst.* **2015**, *C27*, 3–8.

Disclaimer/Publisher's Note: The statements, opinions and data contained in all publications are solely those of the individual author(s) and contributor(s) and not of MDPI and/or the editor(s). MDPI and/or the editor(s) disclaim responsibility for any injury to people or property resulting from any ideas, methods, instructions or products referred to in the content.